Molecular Pharmacology Fast Forward. Published on August 9, 2019 as DOI: 10.1124/mol.119.116947
This article has not been copyedited and formatted. The final version may differ from this version.

Thyrotropin Receptor: Allosteric Modulators Illuminate Intramolecular Signaling Mechanisms at the Interface of Ecto- and Transmembrane Domain

Patrick Marcinkowski[1], Annika Kreuchwig[1], Sandro Mendieta[1], Inna Hoyer[1], Franziska Witte[1,3], Jens Furkert[1], Claudia Rutz[1], Dieter Lentz[2], Gerd Krause[1*], Ralf Schülein[1]

[1] *Leibniz-Forschungsinstitut für Molekulare Pharmakologie (FMP), 13125 Berlin, Germany*

[2] *Institut für Chemie und Biochemie - Anorganische Chemie, Freie Universität Berlin, 14195 Berlin, Germany*

[3] *Current affiliation: Max Delbrück Center for Molecular Medicine (MDC), 13125 Berlin, Germany*

Molecular Pharmacology Fast Forward. Published on August 9, 2019 as DOI: 10.1124/mol.119.116947
This article has not been copyedited and formatted. The final version may differ from this version.

Running Title: TSHR intramolecular mechanisms illuminated by PAM and NAM

*Corresponding author information:

Gerd Krause, PhD

Leibniz-Forschungsinstitut für Molekulare Pharmakologie (FMP)

Robert-Rössle-Str. 10

13125 Berlin

Phone: (+49) 30 94793 228

E-Mail: GKrause@fmp-berlin.de

Number of text pages: 20

Tables: 0

Figures: 9

References: 49

Words in abstract: 249

Words in introduction: 686

Words in discussion: 1620

Molecular Pharmacology Fast Forward. Published on August 9, 2019 as DOI: 10.1124/mol.119.116947
This article has not been copyedited and formatted. The final version may differ from this version.

Abstract

The large TSH–bound ectodomain of the thyrotropin receptor (TSHR) activates the transmembrane domain (TMD) indirectly via an internal agonist (IA).

The ectodomain/TMD interface consists of converging helix, Cys-Cys-bridge linked IA and extracellular loops (ECL). In order to investigate the intramolecular course of molecular activation, especially details of the indirect activation, we narrowed down allosteric inhibition sites of negative allosteric modulator (NAM) by mutagenesis, homology modeling and competition studies with positive allosteric modulator (PAM).

From the inhibitory effects of NAM S37a on i) chimeras with swapped ectodomain, ii) stepwise N-terminal truncations, iii) distinct constitutively active mutations (CAM) distributed across the hinge region and ECL, but not across the TMD, we conclude that S37a binds at the ectodomain/TMD interface, between the converging helix, ECL1 and the IA. This is also supported iv) by the non-competitive inhibition of PAM-C2-activation by S37a in the TSHR-TMD construct lacking the ectodomain. Mutagenesis studies on the IA and ECL were guided by our refined model of the ectodomain/TMD interface and indicate v) an interaction with the TSHR-specific residues E404 (preceding IA) and H478 (ECL1). At this new allosteric interaction site, NAM S37a blocks both TSH- and PAM-induced activation of the TSHR.

Our refined models, mutations and new allosteric binding pocket helped us to gain more detailed insights into the intramolecular course of TSHR activation at the ectodomain/TMD interface, involving delocalization of the converging helix and rearrangement of the conformation of IA. These changes are embedded between the ECL, and co-operatively trigger active conformations of TMD.

Molecular Pharmacology Fast Forward. Published on August 9, 2019 as DOI: 10.1124/mol.119.116947
This article has not been copyedited and formatted. The final version may differ from this version.

Significance Statement

The intramolecular activation mechanisms of the TSHR appear to be distinct from those of other GPCRs, as it has a uniquely large N-terminal ectodomain, which includes the hormone binding site and an internal agonist sequence. We present new molecular and structural insights into the interface between ectodomain and transmembrane domain in the TSHR, as well as the transfer of activation to the transmembrane domain. This knowledge is critical for understanding activation or inhibition of the receptor by allosteric ligands. We have identified a new allosteric antagonist binding pocket that is located exactly at this interface, and which possesses specific features that may allow the generation of potent highly TSHR-selective drugs, of potential value for the treatment of Graves' orbitopathy.

Molecular Pharmacology Fast Forward. Published on August 9, 2019 as DOI: 10.1124/mol.119.116947
This article has not been copyedited and formatted. The final version may differ from this version.

Introduction

Together with the lutropin and follitropin receptors, the thyrotropin receptor or thyroid-stimulating-hormone (TSH) receptor (TSHR) belongs to the subfamily of glycoprotein hormone receptors (GPHR), the class A G-protein-coupled receptors (GPCRs) (Vassart *et al.*, 2004). TSH binds to its receptor and leads to the stimulation of secondary messenger pathways, predominantly involving cAMP (Laurent *et al.*, 1987). Inositol 1,4,5-trisphosphate (IP_3) and diacylglycerol (DAG) pathways are also activated at higher TSH concentrations (Kero *et al.*, 2007; Song *et al.*, 2010). TSH and the TSHR are key proteins in the control of thyroid function. TSHR is expressed in the thyroid gland but also in retro-orbital fibroblasts. Pathological activation of the TSHR by autoimmune antibodies that mimic its natural hormone ligand (Rapoport *et al.*, 1998), leads i) to uncontrolled production of thyroid hormones by the thyroid gland, causing hyperthyroidism (Graves' disease, GD) and ii) in the eye to exophthalmos (Graves' Orbitopathy, GO). Antithyroid drugs available on the market inhibit thyroid hormone synthesis in the thyroid gland, but do not act directly on the TSHR and are therefore less effective in the treatment of GO (Sato *et al.*, 2015). Small molecules acting directly on the TSHR are thought to interact allosterically in the transmembrane domain (TMD) as positive and negative allosteric modulators (PAM, NAM)) (reviewed in (Krause and Marcinkowski, 2018)).

The molecular activation mechanisms of TSHR appear to be distinct from that of other GPCRs due to its unique large N-terminal extracellular domain (ECD) in terms of overcoming its inhibitory function (Zhang *et al.*, 1995, 2000; Vlaeminck-Guillem *et al.*, 2002) upon ligand binding (Kleinau *et al.*, 2011). The hormone TSH binds between the two distinguishable receptor parts of the ECD, the leucine-rich repeat domain (LRRD) and the hinge region (reviewed in (Krause *et al.*, 2012)). It is hypothesized that this binding triggers conformational changes at a common convergent center of the LRRD and hinge region that then dissolve the inherent tethered inhibition by the ECD (reviewed in (Kleinau *et al.*, 2017)). A recent peptide screening study identified an internal agonist

sequence (TSHR 405-414) which is a highly conserved sequence shortly prior to TMH1 in GPHR (Brüser *et al.*, 2016). A schematic overview of the nomenclature and topology of TSHR is shown in Figure 1.

For GPHR, only structure fragments for LRRD with bound stimulating (TSHR 21-260, PDB: 3G04) (Sanders *et al.*, 2007) and blocking antibodies (TSHR 22-260, PDB: 2XWT) (Sanders *et al.*, 2011) and of bound FSH on LRRD and the hinge region (FSHR 18-359, PDB 4AY9) (Jiang *et al.*, 2012) are available. Molecular homology models of TSHR have therefore been assembled by variant fragments of the ECD and the transmembrane domain (TMD) using diverse templates (Kleinau *et al.*, 2017).

Single point constitutively activating mutations (CAM) in the transition of LRRD to hinge region on the converging helix (CH) and in the ECL of TSHR showed synergistic effects in their combinations as multiple mutations and cooperatively trigger the signal (Kleinau *et al.*, 2008). These and many other CAM (collected in GPHR research resource: www.ssfa-gphr.de (Kreuchwig *et al.*, 2013)) support the hypothesis that the hinge region interacts with the ECL constraining the basal state, which is released/changed upon activation (in depth reviewed for FSHR by Briet et al. (Briet *et al.*, 2018).

Nonetheless, due to the lack of the crystal structure of the overall receptor, it is not clear i) how ECD and TMD are arranged relative to each other and ii) how the indirect activation of the TMD takes place in detail and iii) whether and how PAM and NAM act on this activation.

Based on the mentioned previous findings and by combining mutagenesis, modeling and small ligand modulators, we aim to shed light on these critical points. We have studied the effect of our recently discovered highly TSHR selective small molecule NAM S37 as racemate and its active enantiomer S37a (Marcinkowski *et al.*, 2019) i) on stepwise N-terminally truncated TSHR constructs, ii) on the TMD alone and iii) on point mutations distributed across the hinge region, all

three ECL and the TMD. The TSHR constructs were activated either by TSH and/or by a small molecule PAM - C2 (Neumann *et al.*, 2009, 2016).

Molecular Pharmacology Fast Forward. Published on August 9, 2019 as DOI: 10.1124/mol.119.116947
This article has not been copyedited and formatted. The final version may differ from this version.

Materials and Methods

Generation of TSHR mutants

Unless otherwise specified, all mutants were tagged with green fluorescent protein at the intracellular C-terminus to evaluate expression. pTSHR-GFP (wild type human TSHR cDNA present in the pEGFP-N1 expression vector, Clontech, Heidelberg, Germany) has been described before (Teichmann *et al.*, 2014) and was used as template for the generation of mutants. The sequences of all constructs were verified by Sanger sequencing (Source Bioscience, Berlin, Germany).

Truncated constructs

Ectodomain truncated TSHR constructs (Figure 2 A) KNQK (287-764-TSHR), GFGQ (365-764-TSHR) and EDI (ΔSP-409-764-TSHR) with deleted signal peptide (SP, 1-24-TSHR) were amplified from pTSHR-GFP using standard PCR techniques. In order to facilitate the deletion of the ectodomain fragments, an EcoRI restriction site was introduced between the sequence encoding TSHR amino acid position C24 and S25 directly after the signal peptide cleavage site. Thereby the amino acids G, I and Q were added into truncated and wildtype (wt)-TSHR that were believed to have no influence on the structure and function of the receptor constructs.

In EDI, the signal peptide was deleted by exchange with a fragment of the CMV promoter from pEGFP-N1 using restriction endonucleases SnaBI and EcoRI. An N-terminal FLAG tag was introduced into truncated and wt-TSHR constructs directly ahead of the EcoRI site by overlap extension PCR (Ho *et al.*, 1989).

Chimeras

For TSHR-FSHR chimeras, the sequences of both receptors were exchanged at the conserved region after leucine-rich repeat 11 (YPSHCCAF), in accordance with the T3 and F3 chimeras of Schaarschmidt et al. (Schaarschmidt *et al.*, 2014) and using restriction free cloning (Van Den Ent and Löwe, 2006). They were designated as TSHRxFSHR (**T**SHR-LRRD and **F**SHR-hinge/TMD)

and FSHRxTSHR (**F**SHR-LRRD and **T**SHR-hinge/TMD). An N-terminal FLAG tag after the FSHR signal peptide was introduced into FSHR and FSHRxTSHR by overlap extension PCR according to the truncated TSHR constructs. The C-terminally GFP tagged chimeras were present in the pEGFP-N1 vector. Detailed cloning procedure and primers used will be provided upon request.

Point mutations

Point mutated hTSHR present in the pcDNA3 expression vector were used from lab stock and have been described before (Kleinau *et al.*, 2010). Point mutated hTSHR present in pEGFP-N1 were generated using site-directed mutagenesis, including the proof reading DNA polymerase PfuTurbo (Agilent).

Cell culture and transfection

Human embryonic kidney (HEK 293T) cells (DSMZ, Braunschweig, Germany) were cultivated in Dulbecco's modified Eagle's medium (DMEM, GlutaMax, Thermo Fisher) containing 1 g/l glucose, 10% fetal bovine serum (Biochrom, Berlin, Germany), 100 IU/ml penicillin and 100 µg/ml streptomycin at 37°C in a humidified 5% CO_2 incubator. For transient transfection of HEK 293T cells, a mixture of 1 µg polyethylenimine (PEI) and 0.4 µg plasmid DNA in serum free DMEM was added to cells grown in 24 well plates one day after seeding.

For the generation of HEK 293T cell lines stably expressing the truncated TSHR, transiently transfected cells were treated with 400 µg/ml G418 twice a week. Approximately 4 weeks after transfection, cells were sorted for GFP fluorescence using the BD Aria II cell sorting device (BD biosciences, Erembodegem, Belgium). All cells were routinely tested for mycoplasma infection.

Determination of cell surface expression by flow cytometry

In a 24 well plate, 2×10^5 cells per well were seeded without selection antibiotics. 3 days after seeding, cells were detached with 1 mM EDTA in phosphate buffered saline (PBS) and blocked for 10 minutes in blocking buffer (PBS, 0.5% bovine serum albumin, BSA). All steps were performed at 4°C on ice. The cells were incubated with primary and secondary antibodies for 30

minutes in blocking buffer, respectively. Primary mouse anti-FLAG (clone M2, Sigma) antibody was used diluted 1:1,000 and R-phycoerythrin (PE)-conjugated goat anti-mouse IgG secondary antibody (Jackson ImmunoResearch) was diluted 1:50. Cells were washed with blocking buffer 3 times after each antibody incubation. 10,000 cells per sample were analyzed using a fluorescence flow cytometer (FACSCalibur, BD biosciences) with a 488 nm argon laser. GFP fluorescence was measured at 510±20 nm and PE fluorescence at 585±42 nm bandpass. Each sample was measured in duplicate. The data were analyzed using FCS Express 4 (De Novo Software). Cells were gated in a FSC/SSC dot-plot; transfected cells were gated by positive GFP fluorescence compared to non-transfected HEK 293T cells. Plasma membrane receptors were quantified by mean of PE fluorescence using the log Gaussian fitting algorithm in GraphPad Prism 5. Data points represent mean values of duplicates ± standard deviation, normalized to wt-TSHR. A single experiment is shown which is representative of three independent experiments.

Ligand treatment and determination of intracellular cAMP accumulation

In a 24 well plate coated with poly L-lysine (25 µg/ml, molecular weight ≥300,000, Sigma), 2×10^5 cells per well were seeded. Stable cell lines were seeded without selection antibiotics and ligand treatment was performed 72 hours after seeding. Transiently transfected cells were treated with ligands 48 hours after transfection. Intracellular cyclic adenosine monophosphate (cAMP) accumulation was measured by radioimmunoassay as described previously (Kleinau *et al.*, 2010). Briefly, cells were washed with 1 ml of stimulation buffer (DMEM GlutaMax supplemented with 10 mM HEPES, 0.5% BSA, and 0.25 mM 3-isobutyl-1-methylxanthine (IBMX)) and incubated for 1h at 37°C with stimulation buffer alone or stimulation buffer containing bovine TSH (bTSH, Sigma), recombinant human follitropin (rhFSH, R&D systems) and/or small molecule ligands at the indicated concentrations. Small molecule TSHR ligands - C2 and Antag3 - were a gift from Susanne Neumann and Marvin Gershengorn (NIH, USA). The development of S37-rac. and S37a has been described comprehensively (Marcinkowski *et al.*, 2019).

Radioligand displacement binding assay

The assay was performed using whole cell membranes prepared from HEK 293T cells stably expressing wildtype human TSHR (HEK-TSHR), as described previously (Hoyer, 2014). For each sample, a membrane preparation containing 10 µg total protein and 30,000 cpm ^{125}I-bTSH (Thermo Fisher Scientific TRAK kit, B.R.A.H.M.S, Hennigsdorf, Germany) were incubated with increasing concentrations of cold ligands in a final volume of 200 µl in binding buffer (50 mM Tris, 2 mM EGTA, 10 mM $MgCl_2$, 0.5 g/l BSA, 213 µg/ml bacitracin, 80 µg/ml benzamidine, 17 µg/ml aprotinin, 3 µg/ml soy bean trypsin inhibitor, 0.5 mM phenylmethyl sulfonyl fluoride (PMSF), pH 7.5) for 2 hours at 25°C. Membranes were harvested on GF/C glass fiber filters (Inotech IH-201-C) and washed 5 times with cold PBS. Radioactivity of bound ligand was then measured in a gamma-counter.

Data analysis

The present manuscript is exploratory and does not test a statistical null hypothesis. The individual, independent experiments for cAMP accumulation and radioligand binding were performed in triplicates and for concentration-response curves in duplicates. If not stated otherwise, raw data are shown from a single experiment which is representative of three independent experiments and normalized data are shown as average of three independent experiments. Data were analyzed using the software GraphPad Prism 5 and are shown as mean and standard deviation. For concentration-dependent curves x values were log-transformed and y mean values were fitted using a three-parametric (bottom, top, E/IC_{50}) sigmoidal curve.

Crystal structure determination of S37a

The racemate S37 had been separated into its enantiomers S37a (eluted first) and S37b (eluted second) by chiral HPLC as described previously (Marcinkowski *et al.*, 2019).

Crystals could be obtained from a super-saturated solution of S37a in 1,4-dioxane. Diffraction data were collected on a Bruker-AXS D8 Venture instrument equipped with an Incoatec Microfocus

Source using Cu Kα radiation and a Photon detector. The APEX3 software (DOC-M86-EXX229 APEX3 Software User Manual, 2016) was used for data collection and reduction. The structure was solved and refined using SHELXT (Sheldrick, 2015b) and SHELXL (Sheldrick, 2015a), respectively. The absolute configuration of **37a** was unequivocally determined by an X-ray crystal structure analysis by anomalous dispersion with a Flack parameter of 0.037(4). ORTEP for Windows (Farrugia, 1997) was used to create the drawing of the structure.

Homology Modelling

Generation of the TMD model of TSHR in the inactive state started by assembling the best transmembrane helix templates, on the basis of our published fragment-based molecular modeling approach (SSFE, Worth *et al.*, 2017). The loops were generated with the help of the GPCR-I-TASSER web resource (Zhang *et al.*, 2015).

To generate full length models, we updated the previously generated ECD/ TSH complex model (Kleinau *et al.*, 2017) based on the FSHR/FSH crystal structures (4AY9, 4MQW, (Jiang *et al.*, 2012)). The ECD model also contains the hinge region, particularly the short CH and part of the internal agonist. We truncated the last residues P407 and C408 of the ECD so that C284 on CH is accessible. At the TSHR model of the TMD (inactive state), we added a part of the internal agonist $_{408}$CEDIMGY prior to TMH1, using as template the crystal structure of a homologous sequence fragment CENVIGY (PDB: 1DQA). The resulting extended TMD construct now contains a freely accessible C408. For docking the ECD to the TMD, two web tools were used, HADDOCK (van Zundert *et al.*, 2016) and ITASSER (Zhang *et al*., 2015), exploiting the user-specified restraint (inter-residue or distance restraints) of the existing disulfide bond between C284 at CH of the ECD and C408 now being located in the TMD model. Both approaches generated a variety of docking clusters. From the best scoring clusters, we chose for further consideration the one that was predicted in an identical configuration by the two methods.

Molecular Pharmacology Fast Forward. Published on August 9, 2019 as DOI: 10.1124/mol.119.116947
This article has not been copyedited and formatted. The final version may differ from this version.

The crystal structure of S37a (Figure 5) was docked into the TMD-model (corresponding to the EDI construct) of the inactive state using the docking module Glide of the Maestro11 software (Schrödinger, LLC, New York, NY, 2017). Glide docking methodologies use hierarchical filters allowing flexible ligand positioning in the receptor binding-site region. As a first step, the model quality was checked by the Protein Preparation Wizard. Subsequently, a grid defining the shape and properties of the binding site region was set up, based on the previously published characterization of the binding site (Hoyer *et al.*, 2013) of the TSHR TMD. During the docking process, exhaustive ligand torsion sampling and refinement of selected docking poses led to the selection of high affinity, low Glide scoring poses of S37a. Finally, the selected poses were minimized with full ligand flexibility in a post-docking minimization step.

Molecular Pharmacology Fast Forward. Published on August 9, 2019 as DOI: 10.1124/mol.119.116947
This article has not been copyedited and formatted. The final version may differ from this version.

Results

To improve our understanding of the intramolecular course of molecular activation across the entire TSHR, especially details of the indirect activation of the TMD and how this is influenced by NAM, we narrowed down the potential target sites of NAM.

Truncated TSHR constructs

Firstly, three truncated TSHR constructs related to previous reports (Vlaeminck-Guillem *et al.*, 2002) have been generated. They were shortened stepwise by parts of the ECD but retain the TMD. The first truncation TSHR 287-764 (starting with KNQK) lacks the LRRD, but still also contains the entire extracellular hinge region. The second truncated TSHR 365-764 (GFGQ) contains only the second half of the hinge region after the C-peptide, including the internal agonist. The shortest construct, TSHR 409-764 (EDI), only consists of the TMD. In contrast to construct 415-764 (called KFLR in Vlaeminck-Guillem *et al.*, 2002), our EDI also contains 6 preceding amino acids, in order to constitute the complete transmembrane helix 1 (TMH1). (Figure 2A).

Since the N-terminally truncated TSHR-constructs cannot be activated by TSH (Vlaeminck-Guillem *et al.*, 2002), the activation with the small molecule agonist called C2 was a prerequisite for antagonist treatment. The truncations were activated by C2 with different efficacies in transiently transfected HEK 293T cells (Supplemental Figure 1). The EC_{50} of C2-induced cAMP production was 2 µM in KNQK, but 1 µM in wt-TSHR and in the other truncated constructs. This demonstrates the mutant's functionality in terms of G_s activation, which has also been previously shown for the TSHR truncation KFLR (Neumann *et al.*, 2009).

Secondly, stable HEK 293T cell lines expressing the constructs were generated. Their cell surface expression was 8 to 40% of wt-TSHR (Supplemental Figure 2). Constitutive activity for the truncated constructs has been described for analogous constructs (Vlaeminck-Guillem *et al.*, 2002), which we generally confirmed (Supplemental Figure 3A).

Figure 2D shows that all truncated constructs were inhibited by S37, which proves in the first place that it binds to the TMD of TSHR. Moreover, binding to the LRRD was excluded for the active enantiomer S37a by ECD/TMD swapping TSHR-FSHR chimeras (Supplemental Figure 4). The effects of respective hormones on such chimeras have been described previously (Schaarschmidt *et al.*, 2014). S37 and S37a are selective for TSHR and do not inhibit the FSHR. Therefore they should inhibit only the chimera containing the TSHR TMD, as was the case for S37a.

Interestingly, compound S37 had a very different effect in the truncated TSHR than did wt-TSHR. In wt-TSHR, C2 activation was inhibited by 25% using 50 µM S37 (Figure 2C, IC_{50} > 50 µM). However in the truncated constructs C2-induced cAMP signaling was completely inhibited at 50 µM and the IC_{50} was 3 µM for the KNQK and GFGQ and 10 µM for the EDI construct (Figure 2 C, blue and grey curves, respectively).

Although the TSHR ECD is dispensable for S37 binding (activation of EDI is inhibited by S37), the ECD seems to have a strong influence on the function of S37 (Figure 2C), especially in contrast to C2 whose EC_{50} is only changed slightly upon removal of the ECD (Supplemental Figure 1).

In previous studies, competition experiments using full length wt-TSHR revealed competitive inhibition of S37 to TSH for cAMP signaling (Marcinkowski *et al.*, 2019). In order to prove that S37a does not actually displace bTSH, we performed a radioligand binding assay. As expected, we could show that S37a does not inhibit ^{125}I-bTSH binding to TSHR (Figure 3).

Moreover, S37 showed non-competitive antagonism to agonist C2 in the cAMP assay for the full length TSHR (Figure 2D), which was confirmed for the EDI construct that lacks the entire ECD (Figure 2E), demonstrating that S37 binds to the TMD but not at the same binding site as C2. To prove the validity of the competition assay, we repeated it in the EDI construct with the inverse agonist Antag3 (Neumann *et al.*, 2014), which is a derivative of C2 and therefore is supposed to inhibit activation by C2 competitively. Indeed, in contrast to S37 we obtained right-shifted

concentration-response curves of C2 when increasing the Antag3 concentration (Figure 2F), indicating competitive antagonism and hence, overlapping binding sites for C2 and Antag3.

These results clearly demonstrate that the binding site for S37 must be located at the TSHR-TMD, but is different from that of the known allosteric C2 binding site in the TMD.

Effects of S37a on TSHR constitutively activating mutants (CAM)

Since S37 and S37a bind to the TMD but not in the classical pocket like C2, we further considered potential interaction sites of S37a between the extracellular vestibule on the top of the 7TM bundle and the ECD. Therefore we tested the inhibitory effect of S37a on known CAM of TSHR (selected from www. SSFA-gphr.de (Kreuchwig *et al.*, 2013)) located on CH of the hinge region (S281Q), internal agonist (N406D), ECL1 (I486F), ECL2 (I568T, T574A) and ECL3 (V656F). CAM in the hinge region and ECL of TSHR probably change particular interactions between ECD and TMD. CAM on variant positions across the TMD (V421I, Y466A, T574A, D619A, M637W, Y643F and L645V) of TSHR are also thought to track other potential binding sites on TMD. CAM in the TMD indicate positions/residues that are important to stabilize the basal receptor conformation in the wild type receptor and are potential switches for receptor activation (Kleinau *et al.*, 2010, 2017; Hoyer *et al.*, 2013). Therefore, different inhibitory effects of S37a depending on particular CAM location should contribute to understand the molecular course of activation and delineation of the binding site.

It is striking that S37a clearly inhibits highly elevated cAMP production (grey/black, figure 4A) of those CAM of TSHR that are located in i) the converging helix, ii) the internal agonist of the hinge region and iii) the ECL (red in Figure 4B). This suggests that S37a blocks conformational changes of activation in these particular regions located at the interface between ECD and TMD.

In contrast, those CAM that are distributed across the TMD and one located in ECL2 close to TMH5, that cause moderate or slightly elevated cAMP, could not be inhibited by S37a (Figure 4A; green 4B). The observed slight partial agonism of S37a at TSHR-wt is more or less retained,

suggesting that the compound does not, or only to a minor extend, influence CAMs located on the transmembrane helices.

These observations suggest that the site of action of S37a is more likely to be harbored at the interface between hinge region and ECL than in the known GPCR ligand binding pockets between the helices.

Docking of S37a crystal structure into model of the TSHR

The crystal structure of the enantiopure compound S37a containing seven chiral centers was determined by X-ray crystal structure analysis, resulting in a bent structure (Figure 5) that confirmed our previously predicted absolute configuration (4aS,5S,5aR,8aR,9R,9aS,10R)-7,10-diphenyl-5,5a,8a,9,9a,10-hexahydro-5,9-methanothiazolo[5',4':5,6]thiopyrano[2,3-f]isoindole-2,6,8(3H,4aH,7H)-trione (Marcinkowski *et al.*, 2019).

Although the TMD model of TSHR construct EDI lacks the entire ECD in the inactive state, NAM S37a was docked into it because truncation mutations demonstrate the inhibitory interaction of S37a even in the TMD alone. Since the N-terminal residues $_{409}$EDIMGY are part of the internal agonist, we used for it a homologous sequence fragment from the crystal structure (PDB 1DQA) as corresponding template prior to TM1. In the truncated EDI construct, the largely accessible extracellular vestibule between TMH1, 2, 3 and 7 is constricted by residues EDIMGY, where E409 and D410 in our model are located along ECL3 in the vicinity to Y643 (TMH6) and K660 (TMH7) respectively. The residues I411, M412 are embedded in the extracellular vestibule by hydrophobic residues on TMH7, TMH1, TMH2 and ECL2 (I568).

Our highest scored docking pose of S37a into the binding cavity of the truncated EDI construct is covered by the internal agonist (fragment), TMH2 (H478), ECL1 (I486) and ECL2 (Figure 6). This is supported by the suppressing effects on particular CAM (Figure 4), whose positions I486 in ECL1 and partly I568 in ECL2 spatially cover the binding site of S37a (indicated by * in Figure 6).

The binding site between TMH1, 2, 3 and the internal agonist (Figure 6) does not overlap with the allosteric binding pocket of C2 (dark blue, Figure 6), which is consistent with the non-competitive inhibitory effect of S37a on the truncated TSHR constructs.

As template for the ectodomain model of TSH/TSHR, the FSH bound fragment of FSHR ectodomain crystal structure (PDB: 4MQW_B) was used. At its C-terminal end, this contained the CH and part of the internal agonist, which are linked by the conserved disulfide bridge (C283-C408).

For the refined ECD/TMD interface, the full length TSHR inactive state model (Figure 7A) shows that CH interacts with ECL1 and that the residues S281 (CH) and I486 (ECL1) are therefore spatially very close to each other. CH is covalently linked via a disulfide bridge to the internal agonist embedded between ECL2 and ECL3 (Figure 7B). Moreover, the full length TSHR model indicates that S37a is therefore immersed in a similar pocket to that in the model of the EDI-TSHR construct. However, in this case S37a interacts additionally with the CH (S281* CAM), E404 and residues of the internal agonist (F405, N406*) (Figure 7C), which are missing in the EDI-TSHR model. TSHR positions S281* (CH), N406* (internal agonist), I486 *(ECL1), I568* (ECL2), V656* (ECL3), whose CAM* (visualized as spheres in Figure 7 B) are in close vicinity to S37a, can be suppressed by S37a (Figure 4).

Effects of S37a on selected mutants near ECL and internal agonist

The binding site model was used for the selection of additional site directed mutations.

Seven different point mutated TSHR variants (Figure 8 B) were generated that were located in close proximity to one of the predicted S37a docking poses and cAMP signaling was investigated. All mutants could be activated by bTSH (Supplemental Figure 5) and were subsequently treated with S37a. Figure 8 A clearly shows that the two mutants E404A and H478A were not inhibited by S37a, whereas in Y414A, Y414F, E480A, and S657A the antagonistic effect is about 60 % at 100 µM S37a, which is similar to wt-TSHR. In S567A, the compound showed only 36 % inhibition

Molecular Pharmacology Fast Forward. Published on August 9, 2019 as DOI: 10.1124/mol.119.116947
This article has not been copyedited and formatted. The final version may differ from this version.

of cAMP accumulation at 100 μM. These results indicate that the two TSH-specific residues E404 and H478 and possibly S567 are critical contact points for S37a.

Molecular Pharmacology Fast Forward. Published on August 9, 2019 as DOI: 10.1124/mol.119.116947
This article has not been copyedited and formatted. The final version may differ from this version.

Discussion

In order to reveal molecular details of how activation is conveyed at the ECD /TMD interface, we have used TSHR-wt and truncated TSHR constructs to investigate details of the indirect and direct activation mechanism of the TMD by TSH, CAM and PAM C2 and studied how this is blocked by the negative allosteric modulator NAM S37a.

In a previous study, Schild plot analyses of TSHR signaling indicated that S37 is a competitive antagonist for TSH stimulation of cAMP. On the other hand, NAM S37a appeared to be a non-competitive antagonist of β-arrestin 1 recruitment, which could mean that S37a binds at the TSHR ECD (Marcinkowski *et al.*, 2019).

Narrowing down the binding site of S37a

In reviewing this assumption, we were able to prove by LRRD and hinge/TMD swapping of TSHR/FSHR chimeras and stepwise N-terminal truncations that the LRRD and hinge region of TSHR are dispensable for S37a binding. In addition, a radioligand binding study proved that ^{125}I-bTSH could not be displaced by S37a (Figure 3 B). Instead, the previously observed competition of S37 and TSH (Marcinkowski *et al.*, 2019) must be an indirect effect, probably elicited by interaction of S37 with determinants of the TSHR hinge region.

It has been shown by mutagenesis that PAM C2 binds allosterically at TSHR, inside the TM bundle (Neumann *et al.*, 2009). Its potential binding pocket between TMH3, 5 and 6 (Neumann *et al.*, 2016) is equivalent to the ancestral orthosteric ligand binding site of many GPCRs (Wacker *et al.*, 2017). As NAM S37 non-competitively inhibits activation by C2, one can conclude that S37a binds elsewhere and does not bind into this particular pocket in the TMD. As inhibition with S37 was also possible in the truncated TSHR containing only the TMD, the presence of a second allosteric binding site within the TMD was conceivable. Moreover, we show here that wild type and truncated TSHR constructs are activated by C2 with similar EC_{50} (Supplemental Figure 1), which implies

that C2 activates the receptor without involvement of the TSHR-ECD - as its absence does not change the affinity of C2.

We assumed that S37a might bind to a non-canonical receptor site similar to one of those that have been recently discovered for ligands on other GPCRs, for example at an intracellular site or at the interface between TMH and membrane (reviewed in (Wacker *et al.*, 2017)). Therefore the inhibitory effect of S37a on CAM was investigated not only on positions in the hinge region, but also on positions distributed across the entire TMD, including intracellular sites. In this context, it should be noted that CAM may not only have direct effects via the mutant residue, but may also have indirect effects on conformations elsewhere in the receptor. Therefore, we have differentiated constitutive mutations only between those in which S37a inhibits or does not inhibit (see Figure 4). It is interesting that this differentiation also discriminates between extracellular and transmembrane mutant residues.

S37a suppressed elevated cAMP of CAM-positions located in the hinge and the extracellular loop only, but had no such effects on CAM positions located in the remaining TMD. Therefore S37a seems to interact at the interface of ECD and TMD rather than on intracellular or membrane interfacial sites.

Verifying new allosteric binding site for NAM S37a at the interface between ECD and TMD

Our homology model of the TSHR TMD suggests a binding site for the NAM S37a among the extracellular loops in the vestibule between TMH 1, 2, 3 and the internal agonist (Figure 6). This is distant from the binding site of PAM C2, which is located deeper in the TMD in between TMH 3, 5, 6 (Neumann *et al.*, 2016). The binding site is consistent with the inhibitory effect of S37 on the different truncated constructs. Any uncertainties about the absolute configuration of the active enantiomer S37a could be cleared up by X-ray crystallography of the compound that was used for docking.

However, the NAM S37a occupies a hitherto unknown allosteric pocket at the ECD/TMD interface which is not related to the established allosteric binding pocket of TSHR nor to the corresponding common orthosteric binding pocket of other GPCRs of the rhodopsin family (reviewed in (Wacker *et al.*, 2017).

The possibility that a NAM could bind in the ECD/TMD interface even near the internal agonist can also be assumed from the fact that the internal agonist as isolated peptide FNPCEDIMGY activates the GPHR, albeit at very high concentrations (Brüser *et al.*, 2016).

Our refined full length TSHR model substantiates the existence of a binding pocket for NAM S37a at the ECD/TMD interface, where S37a interacts with E404 (prior internal agonist), and H478 (TMH2). Their substitution with alanine abrogates the antagonism of S37a, which indicates loss of the compound's affinity at these points or in close proximity. Moreover, this is strongly supported by the facts that S37a is highly TSHR-selective (Marcinkowski *et al.*, 2019) and that residues E404 and H478 are both TSHR specific (see http://www.ssfa-gphr.de/alignment.php).

Other previous experimental findings support the modeled binding site of S37a. The aromatic rings of S37a are surrounded by aromatic residues Y279 (CH), F405 (internal agonist) and Y481 (TMH2/ECL1) which were demonstrated as essential for TSHR functionality (Jaeschke *et al.*, 2006; Mueller *et al.*, 2006). This is also valid for residue I486 on ECL1 (Figure 7B), which can be constitutively activated by mutations (Kleinau *et al.*, 2008).

Course of intramolecular activation mechanism at the ECD / TMD interface

Homology models of the entire TSHR and mutation data suggest an important role for the converging helix (CH, 280-288) when it acts as a pivot of the hinge region during the molecular activation mechanism. The CH is fastened via disulfide bridges (Ho *et al.*, 2001, 2008) (for LHR (Bruysters *et al.*, 2008)) on one side (Cys283–C398) to the additional 13th beta strand that extends the beta sheet of the LRRD and on the other side (C284-C408) to the internal agonist (405-414, (Brüser *et al.*, 2016)).

Molecular Pharmacology Fast Forward. Published on August 9, 2019 as DOI: 10.1124/mol.119.116947
This article has not been copyedited and formatted. The final version may differ from this version.

CH and the internal agonist sequence are both embedded in between the ECLs of the seven TMH (reviewed in (Kleinau *et al.*, 2017; Krause and Marcinkowski, 2018)). According to our own and other molecular models of TSHR (Kleinau and Vassart, 2017), CH interacts with ECL1, as is also supported by the strong CAM of S281Q (located at CH) and I486F (located at ECL1) (Figure 7B). It has previously been suggested that the functionally significant Ser281 interacts with the ECL1 (Jaeschke *et al.*, 2006), as is supported by cross-linking studies (Schaarschmidt *et al.*, 2016). Our NAM S37a is also able to abrogate the CAM N406D (internal agonist), I568T (ECL2) and V656F (ECL3). This reflects the cooperativeness of the three ECL, as previously described (Kleinau *et al.*, 2008), and now additionally illustrates their interrelationships to the CH and the internal agonist. According to our refined TSHR model, the complete internal agonistic sequence is arranged between all three loops and is even embedded between the outmost parts of TMH 1, 2, 3 and 7 (Figure 6 and Figure 7 B, C).

It is conceivable that positions of wt-TSHR with the described CAM influence close interaction between ECD and TMD in the wt-TSHR. Such CAM loosen this tight interaction and may allow higher affinity binding of S37a in these TSHR mutants, which could explain the strong inhibition of CAM located in the ECL, CH and internal agonist but not of those CAM in the seven TMH.

Each described single CAM at the ECD/TMD interface probably changes its spatial location, emphasizing delocalization of CH that also leads, due to the covalent links, to a conformational change or displacement of the internal agonist. Additionally our models suggest that residues of the internal agonist E409 and/or D410 might interact with TMH6 and TMH7, rearranging the transmembrane-spanning helices, especially TMH 6 and 7, and thus allowing the intracellular interaction with G_s protein. Charge interaction of E409 with the highly conserved K660 (TMH7) is conceivable (Figure 6, Figure 7 C), since a single peptide of the internal agonist FNPC**K**DIMGY, wherein glutamate corresponding to E409 is mutated to lysine, blocks GPHR activation (Brüser *et al.*, 2016).

Molecular Pharmacology Fast Forward. Published on August 9, 2019 as DOI: 10.1124/mol.119.116947
This article has not been copyedited and formatted. The final version may differ from this version.

In summary and on the basis of our model-guided mutations and their effects on the function of our NAM S37a, we suggest the following course for the mechanism of the intramolecular activation within TSHR: It is initiated by binding of the hormone TSH between LRRD and the hinge region of the ectodomain. At the ECD /TMD interface, this leads to rearrangements of both the converging helix and the internal agonist. Both are embedded between the extracellular loops and mediate their conformational changes, which in turn finally trigger the active conformations of the transmembrane helices (cartoons Figure 9 A, B). There is an allosteric pocket between TMHs corresponding to the orthosteric rhodopsin-like ligand pocket of many GPCRs of family A and this allows a PAM, such as agonist C2, to activate the TSHR (Figure 9 C). From the inhibitory effects of NAM S37a on i) ECD swapping chimeras, ii) stepwise N-terminal truncations, iii) distinct CAM and iv) site directed mutants, we conclude that S37a binds to an additional pocket at the ECD/TMD interface, most likely between the converging helix, ECL1 and the internal agonist. Thus S37a is exactly able to block both TSH- and PAM-induced molecular activation of the TSHR (Figure 9 D).

We now provide new molecular and structural insights into the interface between the extracellular domain and the transmembrane domain that is critical for activation or inhibition of the TSHR. Our proposed new allosteric ligand binding pocket is located exactly at this interface and exhibits specific features that may allow the generation of potent drugs that are highly specific to TSHR and which could potentially be used for pharmacological intervention in the difficult to treat Graves' orbitopathy (Bartalena, 2013).

Molecular Pharmacology Fast Forward. Published on August 9, 2019 as DOI: 10.1124/mol.119.116947
This article has not been copyedited and formatted. The final version may differ from this version.

Acknowledgements

We thank Jonas Protze for his help with the refinement of the images showing the S37a docking positions.

Author Contributions

Participated in research design: Schülein, Krause, Marcinkowski

Conducted experiments: Marcinkowski, Mendieta, Hoyer, Furkert

Contributed new reagents or analytic tools: A. Kreuchwig, F. Kreuchwig, Krause, Furkert

Performed data analysis: Marcinkowski, Lentz, Furkert

Wrote or contributed to the writing of the manuscript: Krause, Marcinkowski, Schülein, Lentz, Rutz

References

Bartalena L (2013) Graves' Orbitopathy: Imperfect Treatments for a Rare Disease. *Eur Thyroid J* **2**:259–269.

Briet C, Suteau-Courant V, Munier M, and Rodien P (2018) Thyrotropin receptor, still much to be learned from the patients. *Best Pract Res Clin Endocrinol Metab* **32**:155–164, Elsevier Ltd.

Brüser A, Schulz A, Rothemund S, Ricken A, Calebiro D, Kleinau G, and Schöneberg T (2016) The activation mechanism of glycoprotein hormone receptors with implications in the cause and therapy of endocrine diseases. *J Biol Chem* **291**:508–520.

Bruysters M, Verhoef-Post M, and Themmen APN (2008) Asp330 and Tyr331 in the C-terminal cysteine-rich region of the luteinizing hormone receptor are key residues in hormone-induced receptor activation. *J Biol Chem* **283**:25821–25828.

DOC-M86-EXX229 APEX3 Software User Manual (2016) , Springer-Verlag, Berlin/Heidelberg.

Farrugia LJ (1997) ORTEP -3 for Windows - a version of ORTEP -III with a Graphical User Interface (GUI). *J Appl Crystallogr* **30**:565–565.

Farrugia LJ (2012) *WinGX* and *ORTEP for Windows* : an update. *J Appl Crystallogr* **45**:849–854.

Ho SC, Goh SS, Li S, Khoo DH, and Paterson M (2008) Effects of Mutations Involving Cysteine Residues Distal to the S281HCC Motif at the C-Terminus on the Functional Characteristics of a Truncated Ectodomain-Only Thyrotropin Receptor Anchored on Glycosylphosphatidyl-Inositol. *Thyroid* **18**:1313–1319.

Ho SC, Van Sande J, Lefort A, Vassart G, and Costagliola S (2001) Effects of mutations involving the highly conserved S281HCC motif in the extracellular domain of the thyrotropin (TSH) receptor on TSH binding and constitutive activity. *Endocrinology* **142**:2760–2767.

Ho SN, Hunt HD, Horton RM, Pullen JK, and Pease LR (1989) Site-directed mutagenesis by overlap extension using the polymerase chain reaction. *Gene* **77**:51–59.

Hoyer I (2014) Struktur – Funktionsanalysen intramolekularer Signalisierungsmechanismen und pharmakologische Intervention am Thyreoidea-stimulierenden Hormon Rezeptor, Freie Universität Berlin.

Hoyer I, Haas A-K, Kreuchwig A, Schülein R, and Krause G (2013) Molecular sampling of the allosteric binding pocket of the TSH receptor provides discriminative pharmacophores for antagonist and agonists. *Biochem Soc Trans* **41**:213–217.

Jaeschke H, Neumann S, Kleinau G, Mueller S, Claus M, Krause G, and Paschke R (2006) An aromatic environment in the vicinity of serine 281 is a structural requirement for thyrotropin receptor function. *Endocrinology* **147**:1753–1760.

Jiang X, Liu H, Chen X, Chen P-H, Fischer D, Sriraman V, Yu HN, Arkinstall S, and He X (2012) Structure of follicle-stimulating hormone in complex with the entire ectodomain of its receptor. *Proc Natl Acad Sci* **109**:12491–12496.

Kero J, Ahmed K, Wettschureck N, Tunaru S, Wintermantel T, Greiner E, Schütz G, and Offermanns S (2007) Thyrocyte-specific G q / G 11 deficiency impairs thyroid function and prevents goiter development. *J Clin Invest* **117**:2399–2407.

Kleinau G, Haas A-K, Neumann S, Worth CL, Hoyer I, Furkert J, Rutz C, Gershengorn MC, Schulein R, and Krause G (2010) Signaling-sensitive amino acids surround the allosteric ligand binding site of the thyrotropin receptor. *FASEB J* **24**:2347–2354.

Kleinau G, Jaeschke H, Mueller S, Raaka BM, Neumann S, Paschke R, and Krause G (2008) Evidence for cooperative signal triggering at the extracellular loops of the TSH receptor. *FASEB J* **22**:2798–808.

Kleinau G, and Krause G (2009) Thyrotropin and homologous glycoprotein hormone receptors: structural and functional aspects of extracellular signaling mechanisms. *Endocr Rev* **30**:133–151.

Kleinau G, Mueller S, Jaeschke H, Grzesik P, Neumann S, Diehl A, Paschke R, and Krause G (2011) Defining structural and functional dimensions of the extracellular thyrotropin receptor region. *J Biol Chem* **286**:22622–22631.

Kleinau G, Neumann S, Grüters A, Krude H, and Biebermann H (2013) Novel insights on thyroid-stimulating hormone receptor signal transduction. *Endocr Rev* **34**:691–724.

Kleinau G, Worth CL, Kreuchwig A, Biebermann H, Marcinkowski P, Scheerer P, and Krause G (2017) Structural-functional features of the thyrotropin receptor: A class A G-protein-coupled receptor at work. *Front Endocrinol (Lausanne)* **8**.

Kleinau G, and Vassart G (2000, updated 2017) *TSH Receptor Mutations and Diseases*, MDText.com, Inc.; 2000-2017, South Dartmouth.

Krause G, and Marcinkowski P (2018) Intervention Strategies into Glycoprotein Hormone Receptors for Modulating (Mal-)function, with Special Emphasis on the TSH Receptor. *Horm Metab Res* **50**:894–907.

Kreuchwig A, Kleinau G, and Krause G (2013) Research Resource: Novel Structural Insights Bridge Gaps in Glycoprotein Hormone Receptor Analyses. *Mol Endocrinol* **27**:1357–1363.

Laurent E, Mockel J, Van Sande J, Graff I, and Dumont JE (1987) Dual activation by thyrotropin of the phospholipase C and cyclic AMP cascades in human thyroid. *Mol Cell Endocrinol* **52**:273–278.

Marcinkowski P, Hoyer I, Specker E, Furkert J, Rutz C, Neuenschwander M, Sobottka S, Sun H, Nazare M, Berchner-Pfannschmidt U, von Kries JP, Eckstein A, Schülein R, and Krause G (2019) A New Highly Thyrotropin Receptor-Selective Small-Molecule Antagonist with Potential for the Treatment of Graves' Orbitopathy. *Thyroid* **29**:111–123.

Mueller S, Kleinau G, Jaeschke H, Neumann S, Krause G, and Paschke R (2006) Significance of ectodomain cysteine boxes 2 and 3 for the activation mechanism of the thyroid-stimulating hormone receptor. *J Biol Chem* **281**:31638–46.

Neumann S, Huang W, Titus S, Krause G, Kleinau G, Alberobello AT, Zheng W, Southall NT, Inglese J, Austin CP, Celi FS, Gavrilova O, Thomas CJ, Raaka BM, and Gershengorn MC (2009) Small-molecule agonists for the thyrotropin receptor stimulate thyroid function in human thyrocytes and mice. *Proc Natl Acad Sci U S A* **106**:12471–6.

Neumann S, Nir EA, Eliseeva E, Huang W, Marugan J, Xiao J, Dulcey AE, and Gershengorn MC (2014) A Selective TSH Receptor Antagonist Inhibits Stimulation of Thyroid Function in Female Mice. *Endocrinology* **155**:310–314.

Neumann S, Padia U, Cullen MJ, Eliseeva E, Nir EA, Place RF, Morgan SJ, and Gershengorn MC (2016) An enantiomer of an oral small-molecule TSH receptor agonist exhibits improved pharmacologic properties. *Front Endocrinol (Lausanne)* **7**:4–11.

Rapoport B, Chazenbalk GD, Jaume JC, and McLachlan SM (1998) The thyrotropin (TSH) receptor: interaction with TSH and autoantibodies. *Endocr Rev* **19**:673–716.

Sanders J, Chirgadze DY, Sanders P, Baker S, Sullivan A, Bhardwaja A, Bolton J, Reeve M, Nakatake N, Evans M, Richards T, Powell M, Miguel RN, Blundell TL, Furmaniak J, and Smith BR (2007) Crystal Structure of the TSH Receptor in Complex with a Thyroid-Stimulating Autoantibody. *Thyroid* **17**:395–410, Mary Ann Liebert, Inc. 140 Huguenot Street, 3rd Floor New Rochelle, NY 10801 USA.

Sanders P, Young S, Sanders J, Kabelis K, Baker S, Sullivan A, Evans M, Clark J, Wilmot J, Hu X, Roberts E, Powell M, Miguel RN, Furmaniak J, Smith BR, Núñez Miguel R, Furmaniak J, and Rees Smith B (2011) Crystal structure of the TSH receptor (TSHR) bound to a blocking-type TSHR autoantibody. *J Mol Endocrinol* **46**:81–99.

Sato S, Noh JY, Sato S, Suzuki M, Yasuda S, Matsumoto M, Kunii Y, Mukasa K, Sugino K, Ito K, Nagataki S, and Taniyama M (2015) Comparison of efficacy and adverse effects between methimazole 15 mg+inorganic iodine 38 mg/day and methimazole 30 mg/day as initial therapy for Graves' disease patients with moderate to severe hyperthyroidism. *Thyroid* **25**:43–50.

Schaarschmidt J, Huth S, Meier R, Paschke R, and Jaeschke H (2014) Influence of the hinge region and its adjacent domains on binding and signaling patterns of the thyrotropin and follitropin receptor. *PLoS One* **9**:e111570.

Schaarschmidt J, Nagel MBM, Huth S, Jaeschke H, Moretti R, Hintze V, Von Bergen M, Kalkhof S, Meiler J, and Paschke R (2016) Rearrangement of the extracellular domain/extracellular loop 1 interface is critical for thyrotropin receptor activation. *J Biol Chem* **291**:14095–14108.

Sheldrick GM (2015a) Crystal structure refinement with SHELXL. *Acta Crystallogr Sect C, Struct Chem* **71**:3–8, International Union of Crystallography.

Sheldrick GM (2015b) SHELXT – Integrated space-group and crystal-structure determination. *Acta Crystallogr Sect A Found Adv* **71**:3–8, International Union of Crystallography.

Song Y, Massart C, Chico-Galdo V, Jin L, De Maertelaer V, Decoster C, Dumont JE, and Van Sande J (2010) Species specific thyroid signal transduction: Conserved physiology, divergent mechanisms. *Mol Cell Endocrinol* **319**:56–62.

Teichmann A, Gibert A, Lampe A, Grzesik P, Rutz C, Furkert J, Schmoranzer J, Krause G, Wiesner B, and Schülein R (2014) The specific monomer/dimer equilibrium of the corticotropin-releasing factor receptor type 1 is established in the endoplasmic reticulum. *J Biol Chem* **289**:24250–62.

Van Den Ent F, and Löwe J (2006) RF cloning: A restriction-free method for inserting target genes into plasmids. *J Biochem Biophys Methods* **67**:67–74.

van Zundert GCP, Rodrigues JPGLM, Trellet M, Schmitz C, Kastritis PL, Karaca E, Melquiond ASJ, van Dijk M, de Vries SJ, and Bonvin AMJJ (2016) The HADDOCK2.2 Web Server: User-Friendly Integrative Modeling of Biomolecular Complexes. *J Mol Biol* **428**:720–725, The Authors.

Vassart G, Pardo L, and Costagliola S (2004) A molecular dissection of the glycoprotein hormone receptors. *Trends Biochem Sci* **29**:119–126.

Vlaeminck-Guillem V, Ho S-C, Rodien P, Vassart G, and Costagliola S (2002) Activation of the cAMP pathway by the TSH receptor involves switching of the ectodomain from a tethered inverse agonist to an agonist. *Mol Endocrinol* **16**:736–746.

Wacker D, Stevens RC, and Roth BL (2017) How Ligands Illuminate GPCR Molecular Pharmacology. *Cell* **170**:414–427, Elsevier Inc.

Worth CL, Kreuchwig F, Tiemann JKS, Kreuchwig A, Ritschel M, Kleinau G, Hildebrand PW, and Krause G (2017) GPCR-SSFE 2.0 - A fragment-based molecular modeling web tool for Class A G-protein coupled receptors. *Nucleic Acids Res* **45**:W408–W415.

Zhang J, Yang J, Jang R, and Zhang Y (2015) GPCR-I-TASSER: A Hybrid Approach to G Protein-Coupled Receptor Structure Modeling and the Application to the Human Genome. *Structure* **23**:1538–1549.

Zhang M, Tong KPT, Fremont V, Chen J, Narayan P, Puett D, Weintraub BD, and Szkudlinski MW (2000) The extracellular domain suppresses constitutive activity of the transmembrane domain of the human TSH receptor: Implications for hormone-receptor interaction and antagonist design. *Endocrinology* **141**:3514–3517.

Zhang ML, Sugawa H, Kosugi S, and Mori T (1995) Constitutive activation of the thyrotropin receptor by deletion of a portion of the extracellular domain. *Biochem Biophys Res Commun* **211**:205–10.

Molecular Pharmacology Fast Forward. Published on August 9, 2019 as DOI: 10.1124/mol.119.116947
This article has not been copyedited and formatted. The final version may differ from this version.

Footnotes

This work was supported by the Deutsche Forschungsgemeinschaft (DFG, German Research Foundation) [grant number KR1273/4-2].

Molecular Pharmacology Fast Forward. Published on August 9, 2019 as DOI: 10.1124/mol.119.116947
This article has not been copyedited and formatted. The final version may differ from this version.

Figure Legends

Figure 1. Outline of the TSH-receptor's nomenclature and topology of the different domains and features. The extracellular orthosteric binding site of the TSH is located between the leucine rich repeat domain (LRRD) and the hinge region. The latter contains a converging helix (CH) that uses disulfide bridges to link the LRRD and the internal agonist sequence (green) close to the transmembrane domain (TMD). The TMD contains an allosteric binding pocket.

Figure 2. Characterization of the truncated constructs: S37 is a non-competitive antagonist for C2. A) Schematic depiction of TSHR-wt and the stepwise truncation mutants of the N-terminal extracellular domain; i) removal of leucine rich repeat domain (LRRD, beige) yields KNQK, ii) plus removal of half of the hinge region (blue) including the cleavable C-peptide (dashed arrows) yields GFGQ, both also carrying the signal peptide (SP) and iii) removing entire extracellular domain and SP leaving only the transmembrane domain (grey) yields EDI. All constructs contain a C-terminal GFP tag and a Flag tag at the N-terminus after signal peptide cleavage. **B**) Plasma membrane expression of TSHR constructs in stably transfected HEK 293T cells measured as PE fluorescence by flow cytometry after staining with mouse-anti-Flag and PE-conjugated anti-mouse antibodies. **C**) C2 (3 μM) induced cAMP accumulation of wt and truncated TSHR constructs inhibited by S37. **D**) Competition experiments show non-competitive antagonism (lowered maxima) of S37a to C2, in the full-length TSHR and **E**) truncated EDI (TSHR 409-764), which lacks the whole receptor's ectodomain. **F**) Antag3 – a derivative of C2 – is a competitive inhibitor of C2 in EDI.

Figure 3. Radioligand binding study reveals that S37a does not inhibit bTSH binding to TSHR up to a 100 μM concentration. ^{125}I-bTSH (constant 30,000 cpm) and increasing concentrations of non-labeled bTSH (**A**) or S37a (**B**) were incubated with HEK-TSHR membranes.

Figure 4. Constitutively activating mutations (CAM) of the TSHR are either inhibited by S37a, not affected or further activated, depending on their location. A) Transiently

transfected HEK 293T cells were treated with 100 µM S37a (black) or the equivalent amount of DMSO (grey). * indicates Flag-receptor-GFP. All the other receptors are untagged. Columns show mean values of cAMP formation of a single experiment performed in triplicates ± standard deviation. It is representative of two independent experiments. **B**) Scheme of TSHR indicating the locations of CAM that are inhibited by S37a. These are located at the hinge or at the extracellular loops (red). CAM that are not affected (grey) or activated (green) by S37a are located at TMH.

Figure 5: Crystal structure of S37a (orange) in complex with solute 1,4-dioxane (black). The image was generated using the software Ortep3 for Windows v2014.1 (University of Glasgow, (Farrugia, 2012)). Crystallization data were deposited in the Cambridge Crystallographic Data Centre under the CCDC number 1894120.

Figure 6: Docking studies into homology model of the EDI -TSHR construct suggests a binding cavity for the NAM S37a (orange) in the extracellular vestibule among the extracellular loops. This S37a cavity is situated distantly from the binding site of small molecule agonist C2. In contrast to S37a, the allosteric binding pocket of C2 is situated deeper in the TMD (dark blue), where the orthosteric ligand binding pocket is located in many other GPCR of the rhodopsin family. The fragment $_{409}$EDIMGY$_{414}$ of the internal agonist (green) is embedded between ECL3/TMH7 (E409, D410), TMH1/TMH7 (I411), TMH2 (M412) and ECL1 (cyan). S37a is immersed between ECL1, ECL2 (wheaten) and the fragment of the internal agonist. It interacts with H478 and is located between positions I486* (ECL1) and I568* (ECL2) whose CAM (*, see Figure 3) are strongly inhibited by S37a.

Figure 7. Refined full length homology model of the TSHR locked in the inactive state by NAM S37a. A) TSH (pale green) bound between LRRD (beige) and hinge (magenta) with docked NAM S37a (orange) in an allosteric binding site at the newly modeled ECD / TMD interface (boxed). **B**) The converging helix (CH, dark pink) is linked via disulfide bridges with the hinge and the internal agonist (F405-Y414 green). CH interacts with ECL1 (cyan). The internal agonist is

Molecular Pharmacology Fast Forward. Published on August 9, 2019 as DOI: 10.1124/mol.119.116947
This article has not been copyedited and formatted. The final version may differ from this version.

placed between ECL1/ECL2 (F405), ECL2/TMH7-ECL3 (E409, D410) as well as between TMH1 (I411) and TMH2-ECL1 (M412). TSHR positions S281* (CH), I486 *(ECL1), I568* (ECL2 wheaten), V656* (ECL3, salmon), whose CAM* (visualized as spheres) can be suppressed by S37a (Figure 3) are in close proximity to S37a (orange), which **C**) is immersed in a pocket and is also bound by the TSHR specific residues E404 and H478.

Figure 8. Inhibitory effect of S37a on TSHR mutants of model-based selected locations at the extracellular vestibule. A) Inhibition of TSHR-induced cAMP signaling by 20 and 100 µM S37a in percent compared to maximally activated receptor (= 0%). Receptors were activated by approximately the EC_{80} of bTSH (2 mIU/ml in wt-TSHR, Y414F, H478A, E480A and 20 mIU/ml in E404A, Y414A, S567A, S657A). E404A and H478A are not inhibited by S37a, indicating loss of interaction of S37a at these positions. HEK 293T cells were transiently transfected with TSHR constructs containing an extracellular FLAG tag at the N-terminus and an intracellular GFP tag at the C-terminus and two days later treated with bTSH and S37a. **B**) TSHR model showing the location of the investigated mutant residues (green: internal agonist F405-Y414). Clear effects on mutants E404A, H478A support the docking site and TSHR selectivity of S37a (orange).

Figure 9. TSHR cartoons for activation/inhibition signal transmission at ECD/TMD interface. **A**) Unbound basal state; converging helix, CH (magenta) and inverse agonist are covalently linked by disulfide bonds. Both are immersed between the three ECL. **B**) TSH bound between LRRD and sTyr385 of hinge region induce conformational changes of both CH and internal agonist that trigger conformational changes of ECLs and TMHs to the active state. **C**) Allosteric pocket (blue) between TMHs allows small molecule agonist (pale green) to activate the TMD. **D**) An additional allosteric ligand pocket in the extracellular vestibule (yellow) between ECL1, CH and internal agonist allows our NAM S37a (orange) to freeze (red bar) CH and the internal agonist in an inactive conformation, which blocks the activation course of TSH and the PAM as well.

Molecular Pharmacology Fast Forward. Published on August 9, 2019 as DOI: 10.1124/mol.119.116947
This article has not been copyedited and formatted. The final version may differ from this version.

Figures

Figure 1

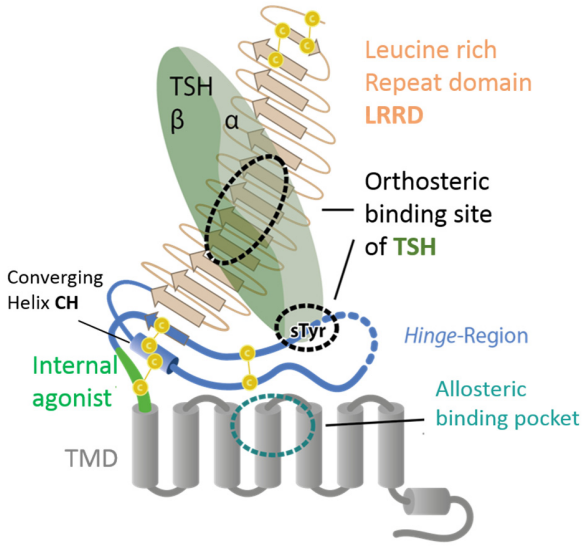

Molecular Pharmacology Fast Forward. Published on August 9, 2019 as DOI: 10.1124/mol.119.116947
This article has not been copyedited and formatted. The final version may differ from this version.

Figures

Figure 2

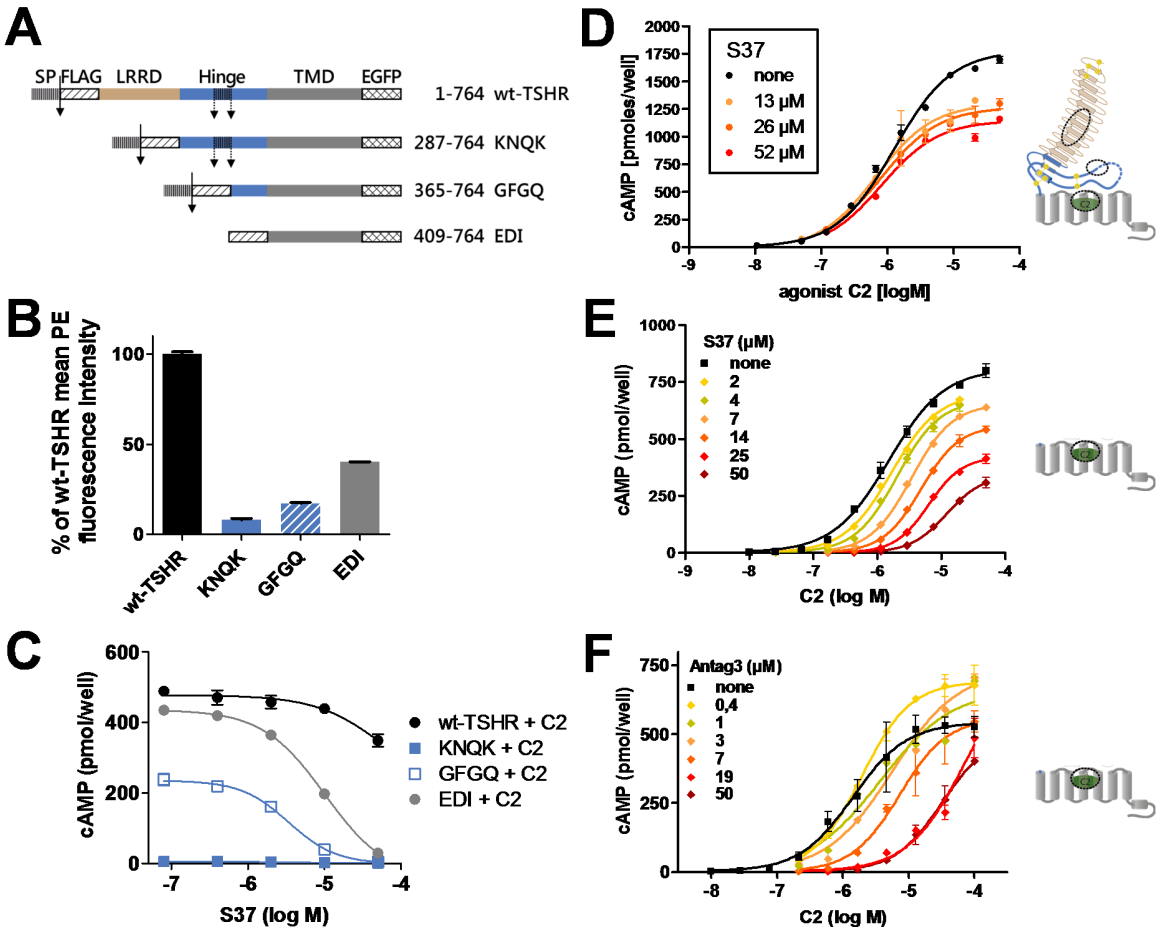

Molecular Pharmacology Fast Forward. Published on August 9, 2019 as DOI: 10.1124/mol.119.116947
This article has not been copyedited and formatted. The final version may differ from this version.

Figures

Figure 3

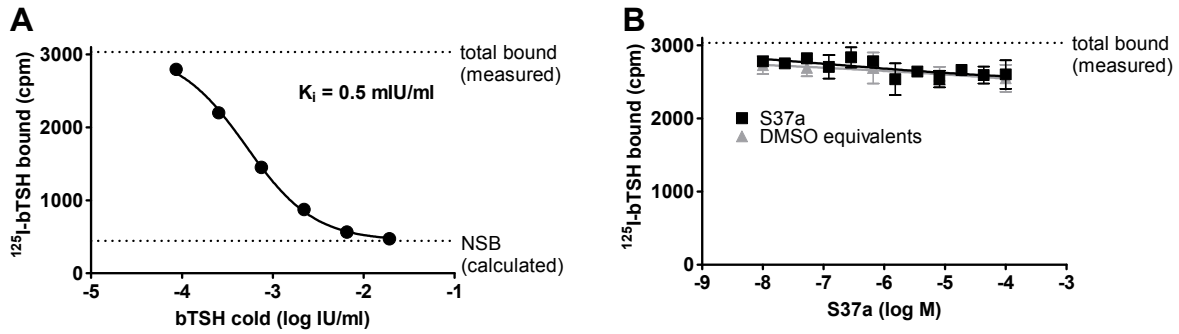

Molecular Pharmacology Fast Forward. Published on August 9, 2019 as DOI: 10.1124/mol.119.116947
This article has not been copyedited and formatted. The final version may differ from this version.

Figures

Figure 4

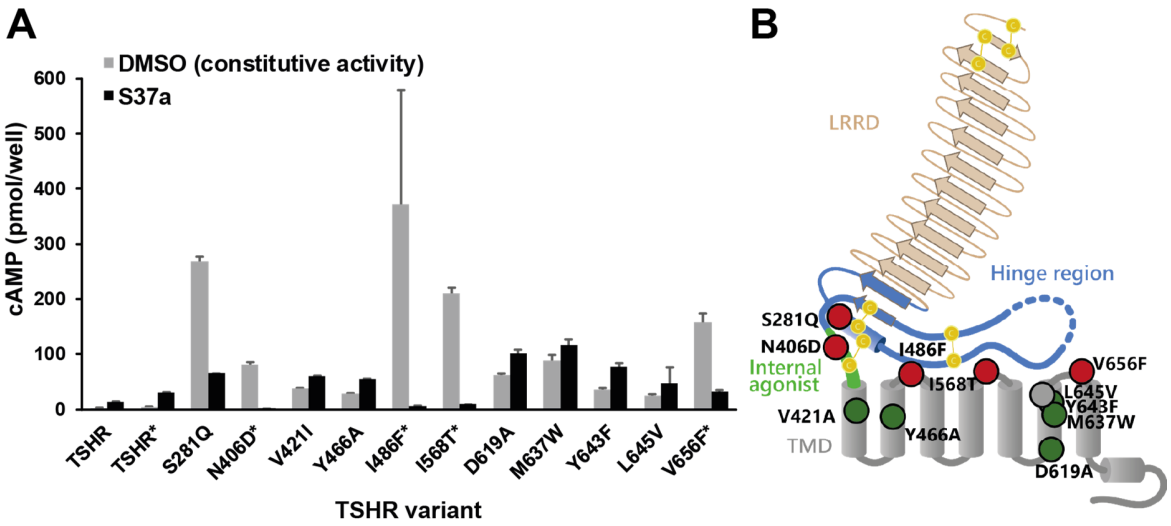

Molecular Pharmacology Fast Forward. Published on August 9, 2019 as DOI: 10.1124/mol.119.116947
This article has not been copyedited and formatted. The final version may differ from this version.

Figures

Figure 5

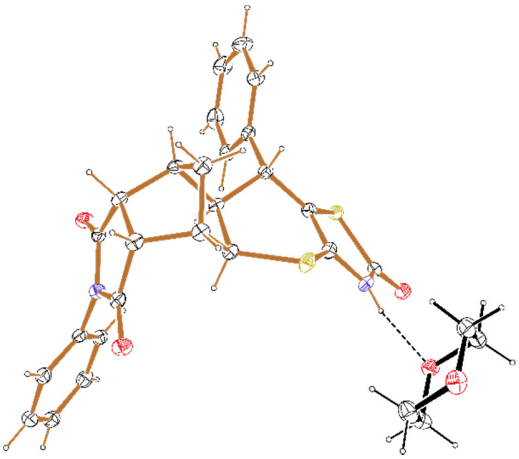

Molecular Pharmacology Fast Forward. Published on August 9, 2019 as DOI: 10.1124/mol.119.116947
This article has not been copyedited and formatted. The final version may differ from this version.

Figures

Figure 6

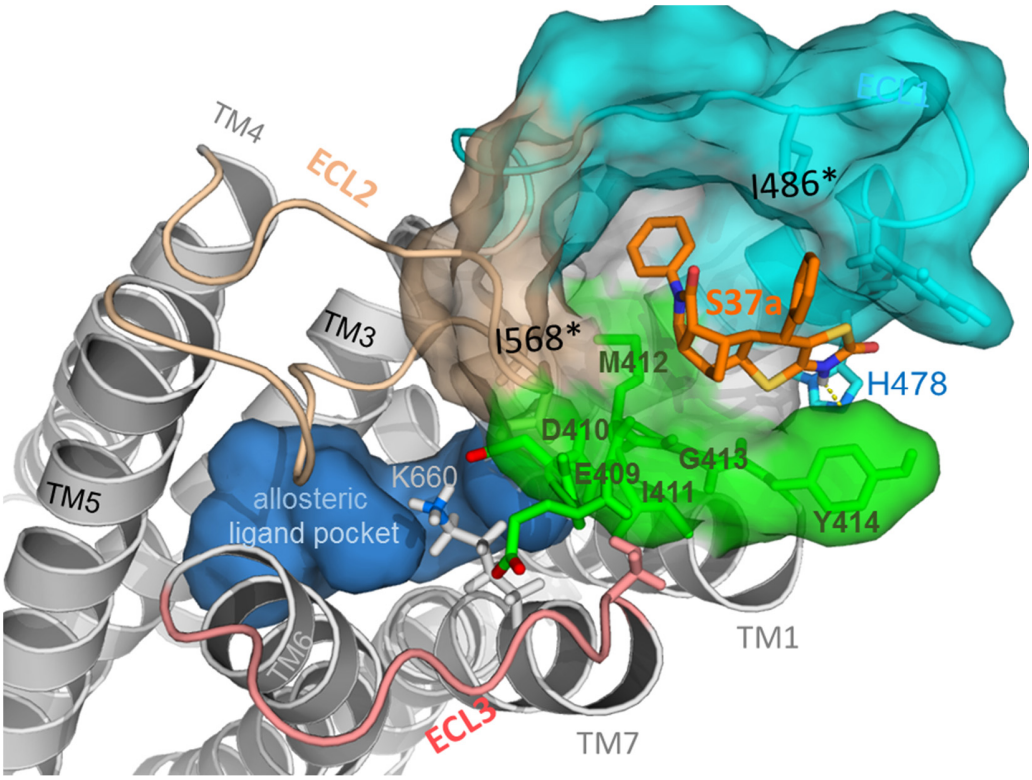

Molecular Pharmacology Fast Forward. Published on August 9, 2019 as DOI: 10.1124/mol.119.116947
This article has not been copyedited and formatted. The final version may differ from this version.

Figures

Figure 7

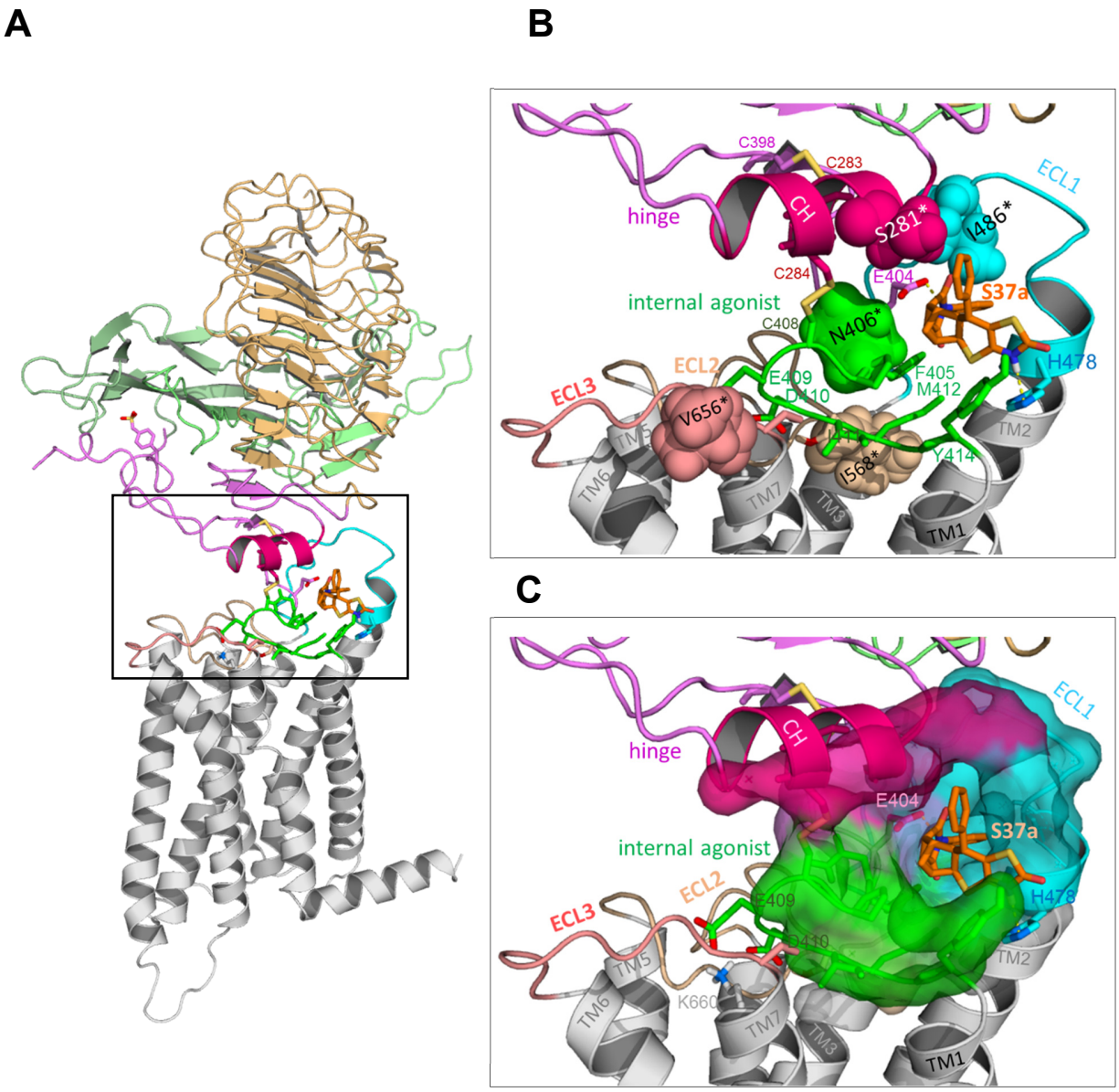

Molecular Pharmacology Fast Forward. Published on August 9, 2019 as DOI: 10.1124/mol.119.116947
This article has not been copyedited and formatted. The final version may differ from this version.

Figures

Figure 8

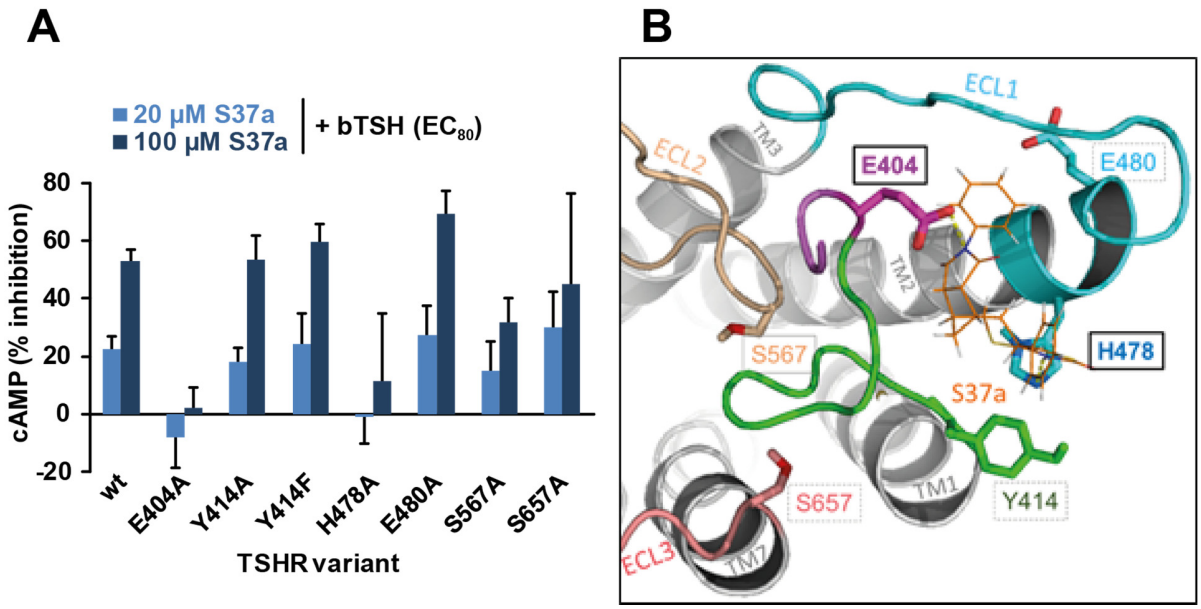

Molecular Pharmacology Fast Forward. Published on August 9, 2019 as DOI: 10.1124/mol.119.116947
This article has not been copyedited and formatted. The final version may differ from this version.

Figures

Figure 9

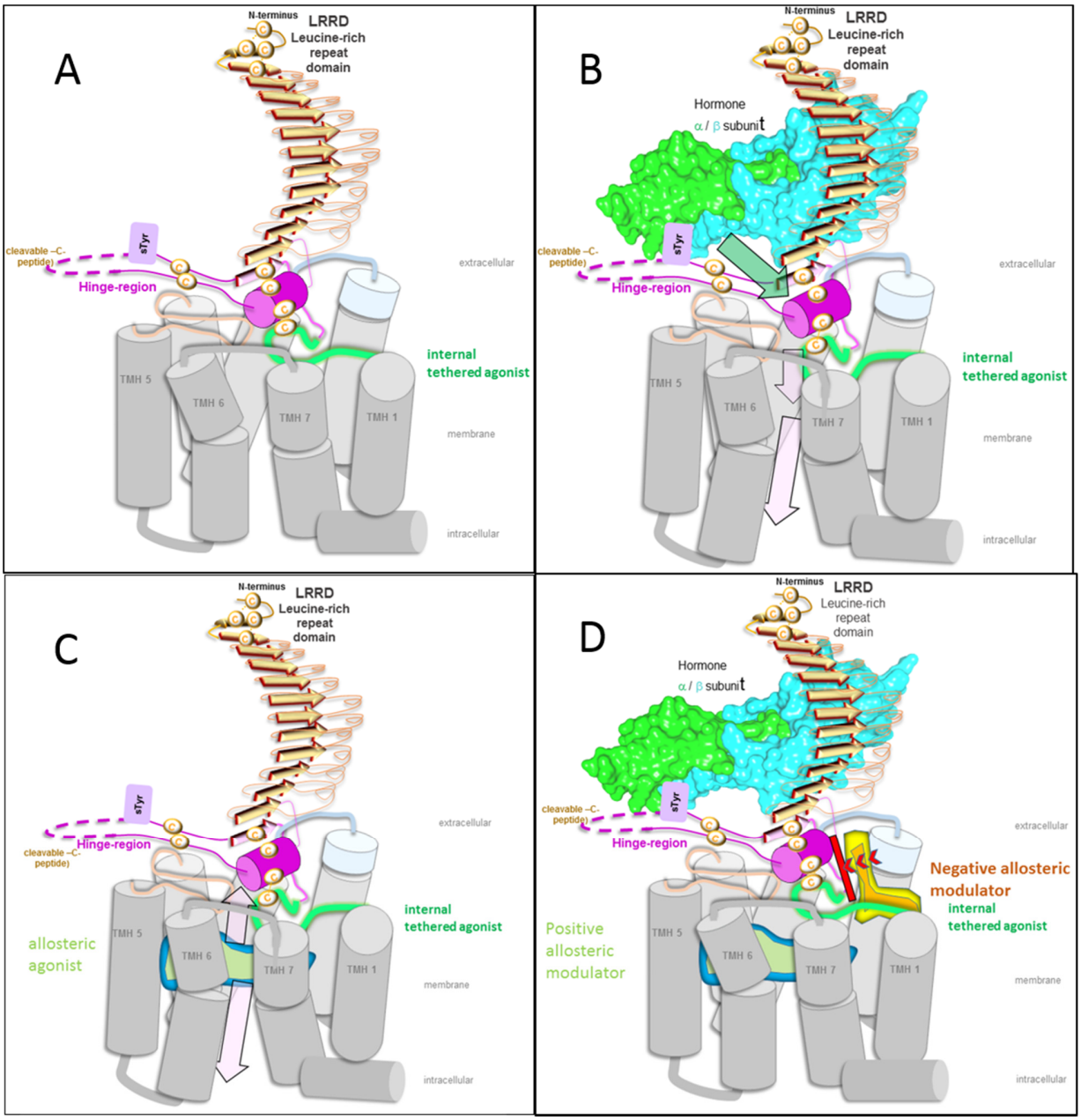

Supplemental Data

Thyrotropin Receptor: Allosteric Modulators Illuminate Intramolecular Signaling Mechanisms at the Interface of Ecto- and Transmembrane Domain

Journal: Molecular Pharmacology

Patrick Marcinkowski[1], Annika Kreuchwig[1], Sandro Mendieta[1], Inna Hoyer[1], Franziska Witte[1,3], Jens Furkert[1], Claudia Rutz[1], Dieter Lentz[2], Gerd Krause[1], Ralf Schülein[1]

[1] Leibniz-Forschungsinstitut für Molekulare Pharmakologie (FMP), 13125 Berlin, Germany

[2] Institut für Chemie und Biochemie - Anorganische Chemie, Freie Universität Berlin, 14195 Berlin, Germany

[3] current affiliation: Max Delbrück Center for Molecular Medicine (MDC), 13125 Berlin, Germany

Supplemental Data

Supplemental Figures

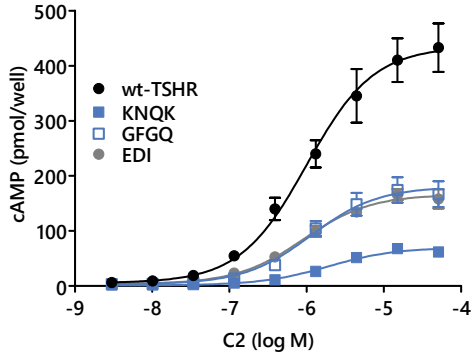

Supplemental Figure 1: Concentration-dependent activation of truncated TSHR by small allosteric agonist C2. The graph shows cAMP accumulation in transiently transfected HEK293 cells.

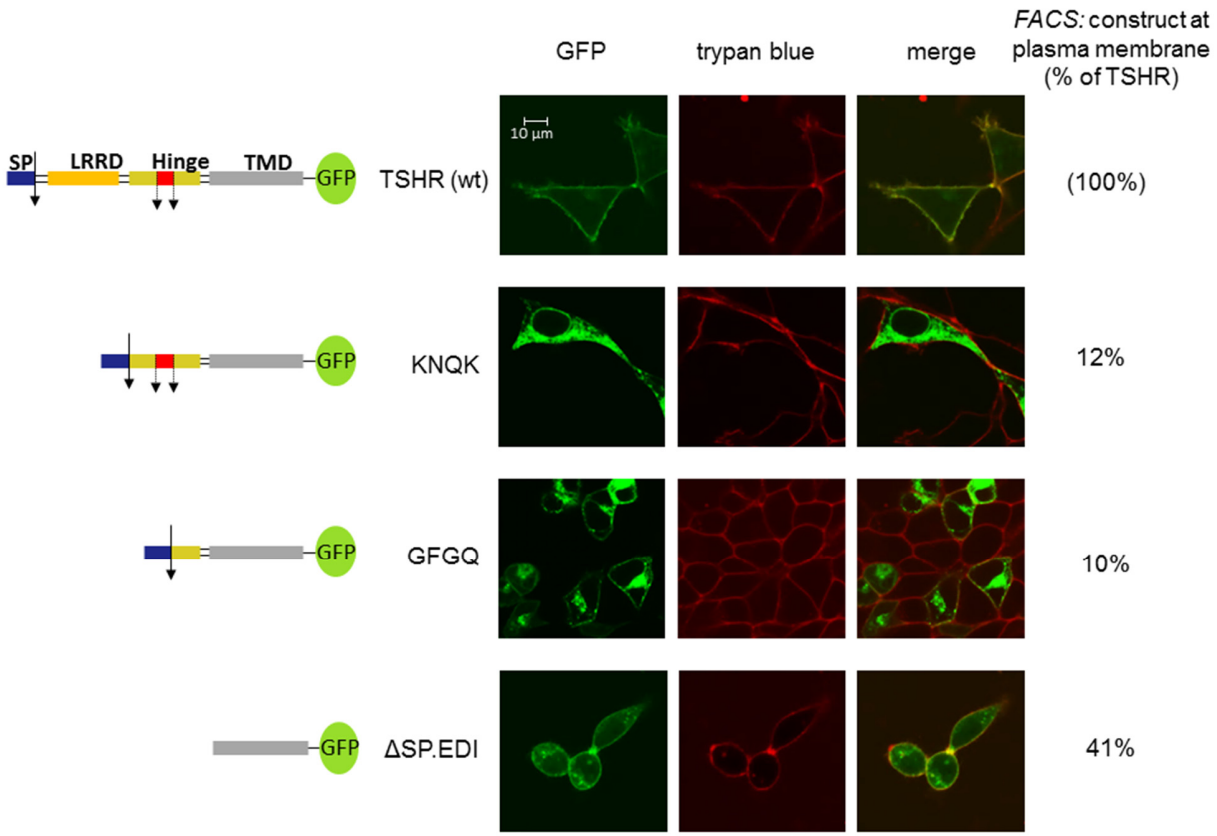

Supplemental Figure 2: Expression of truncated TSHR constructs (scheme, left panel) in transiently transfected HEK293 cells. Expression data by confocal laser scanning microscopy (LSM, 3 central panels) and flow cytometry data (FACS, right panel) of truncated TSHR constructs indicate that the EDI constructs is well expressed on the cell surface in HEK 293T cells although it is lacking the entire ectodomain. Confocal laser scanning microscopy images show the GFP fluorescence signals of the constructs (green) and the trypan blue stained plasma membrane (red). The overlay of green and red channels show yellow color, thus demonstrating the plasma membrane expression of the constructs. $2x10^5$ cells per well were seeded on glass cover slips in 6 well plates. After 24 h of incubation they were transfected

with plasmids containing the TSHR constructs using 1.6 µg polyethylenemimine and 0.8 µg DNA per well. Another 48 h later medium was replaced by PBS and the cells were examined with the microscope ConfoCor2 (Carl Zeiss) using the objective Plan-Apochromat 63x/1.40 Oil DIC (Carl Zeiss) at room temperature. Plasma membranes were stained with a drop of a 0.02 % trypan blue solution put directly into the PBS on top of the cells. GFP signals were visualized using an argon laser (λ_{exc} = 488 nm) and a 505-550 nm bandpass filter, trypan blue using a helium-neon laser (λ_{exc} = 543 nm) and a 560 nm long pass filter. The overlay images were generated using Zeiss LSM Image Browser software version 4.2.0.121. Brightness and contrast was adjusted for all images equally. Flow cytometry (FACS) measurements of the plasma membrane signals of the constructs confirm these results (right panels in % of wt-TSHR). PE fluorescence was measured after staining with mouse-anti-FLAG and PE-conjugated anti-mouse antibodies. Plasma membrane expression of the truncated constructs was substantially lower than that of the wt TSHR and was accompanied by their intracellular accumulation. Most likely, this intracellular retention results from increased misfolding of the truncation mutants which is detected by the quality control system of the early secretory pathway.

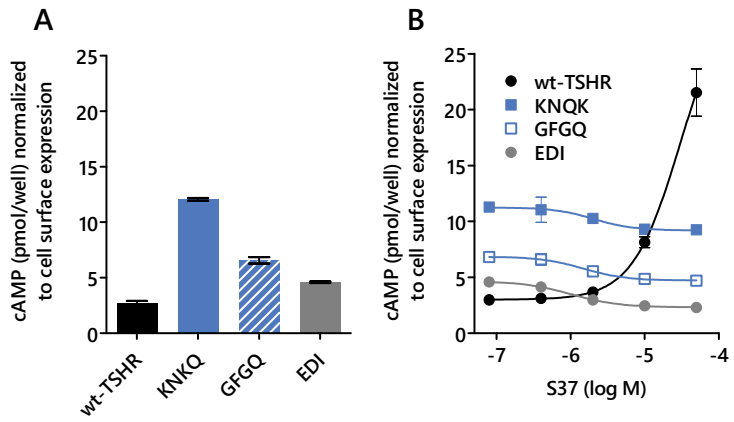

Supplemental Figure 3: Basal activity (A) and effect of S37 alone (B) in truncated TSHR constructs normalized to plasma membrane expression. Basal activity is elevated in truncated TSHR. S37 has a low intrinsic efficacy (E_{max}) for cAMP signaling which means that it activates the wt-TSHR without any other ligand by about 10% of bTSH E_{max}. This effect was completely abolished in the truncated TSHR. On the contrary, it even acts as an inverse agonist by reducing their constitutive activity.

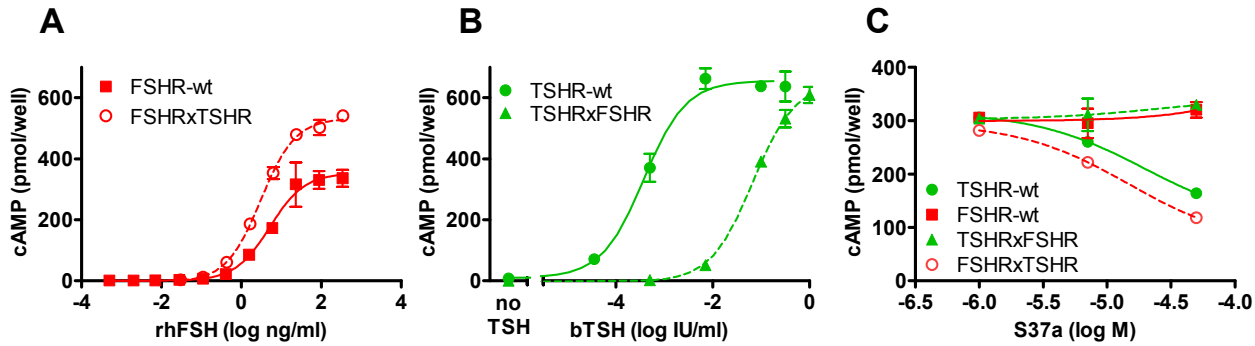

Supplemental Figure 4: cAMP formation mediated by the TSHR-FSHR chimeras. A, B) TSHR/FSHR chimeras which are activated by the respective LRRD-binding hormone (rhFSH→FSHR-LRRD, bTSH→TSHR-LRRD) (also see Schaarschmidt *et al.*, 2014). **C)** Chimera activated with respective EC_{80} of rhFSH (red) and bTSH (green) were inhibited using S37a. S37a is TSHR-selective and does not inhibit FSHR activation, the chimera containing the S37a binding region of TSHR should be inhibited. S37a only inhibits activation of the FSHR-LRRD/TSHR chimera but not that of the TSHR-LRRD/FSHR chimera. These data prove that S37a does not bind at the LRRD of TSHR but instead at the hinge region and/or the TMD.

Supplemental Data

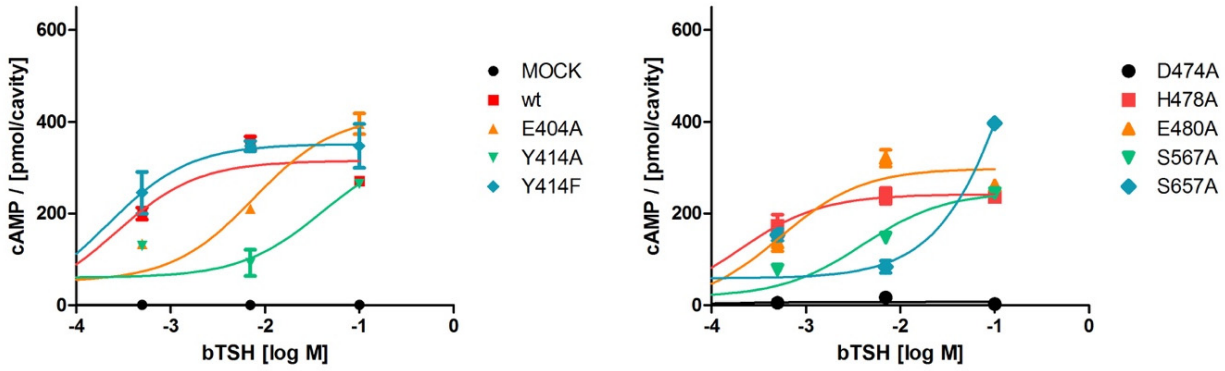

Supplemental Figure 5: cAMP formation mediated by the TSHR variants. Mutant receptor constructs were transiently transfected in HEK 293T cells and activated by bTSH concentration-dependently. cAMP accumulation was induced in all constructs except D474A. The EC_{50} values were elevated in all variants except of Y414F, H478A and E480A.